3D tomographic imaging applied to split cylinder fracture

E. Landis & M. Bridges
University of Maine, Orono, Maine, USA

J. Bolander
University of California, Davis, California, USA

ABSTRACT: In situ 3D imaging experiments were conducted on small split cylinder fracture specimens. Three different materials were considered: a conventional portland cement paste, a fine aggregate mortar, and an ultra high performance concrete. All specimens were scanned using x-ray microtomography, which provided high-resolution 3D images before and after fracture. Quantitative image analysis led to measurements of crack surface area and fragmentation. Results showed that presence of aggregates led to significant fragmentation, and surface area creation.

1 INTRODUCTION

At the scale of the constituents that make up the material, concrete fracture is inherently three-dimensional. This three dimensionality arises because of the spatial distribution of microcracks, the crack branching, and the fragmentation that occurs. Two-dimensional simplifications are typically used because of the simplicity of the analytical formulations, but also due to the lack of good three-dimensional measurements. Towards this latter issue, the work described here is continuation of an ongoing application of a 3D imaging technique, x-ray microtomography, which allows us to examine the microstructural changes that accompany fracture at relatively high resolution.

In this particular project we are interested in the split-cylinder configuration. We chose this because of the experimental convenience of a compressive loading, with the relative simplicity of the stress field. The goal of the work was to quantify the micro fracture characteristics of three widely varying cement-based materials, and to relate those characteristics to measured fracture energy.

2 METHODS AND MATERIALS

2.1 *X-ray microtomography*

The laboratory tool used in this work is called x-ray microtomography. It is similar in practice to conventional medical CT imaging, except that very high spatial resolutions are possible thanks to both the synchrotron radiation source, and a high resolution detector, which make spatial resolutions approaching 1 micron possible (Flannery et al. 1987).

Microtomography has been used to image cement and concrete in a number of applications, including sulfate attack (Stock et al. 2002), porosity and pore structure (Bentz et al. 2000, Lu et al. 2006), and phase distributions (Diamond & Landis 2007). While not as high resolution as electron microscopy, it does offer the advantage of providing true 3D data. Incorporation of an in situ loading frame led to new ways of examining fracture (Landis et al. 1999, Landis et al. 2007) through the examination of the same specimen at progressively higher levels of fracture and damage. Because of the high resolution 3D image data, previously difficult to measure features such as crack branching and crack tortuosity can be quantified.

In the work presented here, imaging was done at the Advanced Photon Source, Beamline 5-BM-C. An illustration of the experimental configuration is shown in Figure 1. At this beamline, a monochromatic, collimated 30 keV x-ray source was used. For each scan, 1500 images were made of the specimen over a rotation of $180°$. Tomographic reconstruction was made using a filtered back-projection algorithm that produced 1299 by 1299 by 800 voxel 16 bit images at 6 microns per voxel side. A photograph of the specimen in the loading frame is shown in Figure 2.

2.2 *Specimens & experimental protocol*

In the experiments described here, materials of three different compositions were examined. The first was a conventional portland cement paste (hardened cement and water), while the second was a mortar that
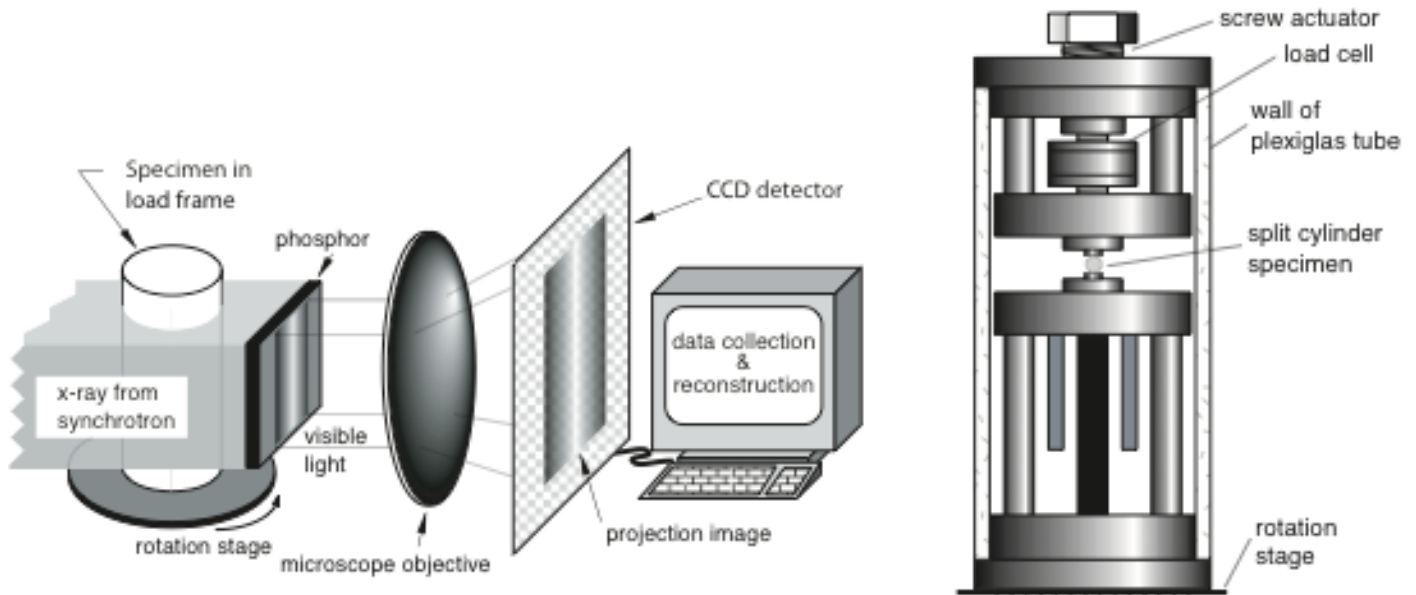
Figure 1. Schematic illustration of microtomography set up (left) and in situ load frame (right).

Figure 2. Photograph of specimen in *in situ* load frame in x-ray beamline. Phosphor scintillator and microscope lens are visible to the right of frame.
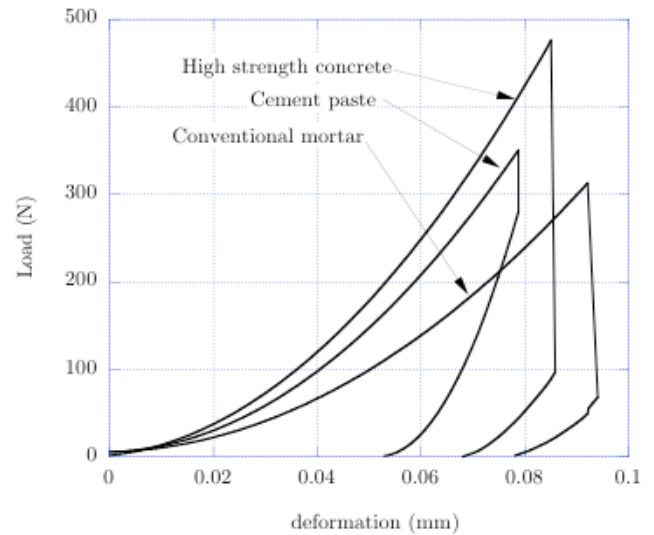

Figure 3. Load-deformation curves for split cylinder tests.

had the same relative amount of cement and water as the paste, but included fine aggregate particles of sizes not exceeding 80 microns. In addition to these conventional materials, an ultra high strength concrete with fine aggregates also not exceeding 80 microns was examined. The objective of the work was to measure the damage and failure patterns in the different materials as they relate to measured strength and the initial composition. Specimens were cylinders with a nominal diameter of 4 mm and a length of 4 mm.

During the experiments, specimens were placed in the loading frame in the x-ray beamline. The experimental protocol was to scan the undamaged specimen, apply a load close to, but not exceeding the failure load, and perform another tomographic scan. A third scan was done after tensile rupture. The bulk load-deformation data for the specimen was recorded during the test.

3 EXPERIMENTS & ANALYSIS

Figure 3 illustrates typical load-deformation curves for the three materials. Qualitatively, the materials do not behave so differently, other than the obvious differences in peak load. Microstructurally, the response of the materials is quite different. Shown in Figure 4 are sample tomographic slices of three different materials after rupture. In the cement paste specimen, with no aggregate particles, we observe relatively simple damage patterns. Crack paths are fairly straight, and the number of fragments generated is small. This result should be compared to both of the specimens containing aggregate particles. In each of these, the crack patterns are complex, and the number of fragments created by the fracture event is significant. These images qualitatively suggest the presence of the aggregate particles facilitate crack stopping, deflection, branching, and other mechanisms that increase the degree of fragmentation. This observation is certainly not new, however, as detailed below, the three dimensional nature of the data allows us to quantify some of our qualitative observations.
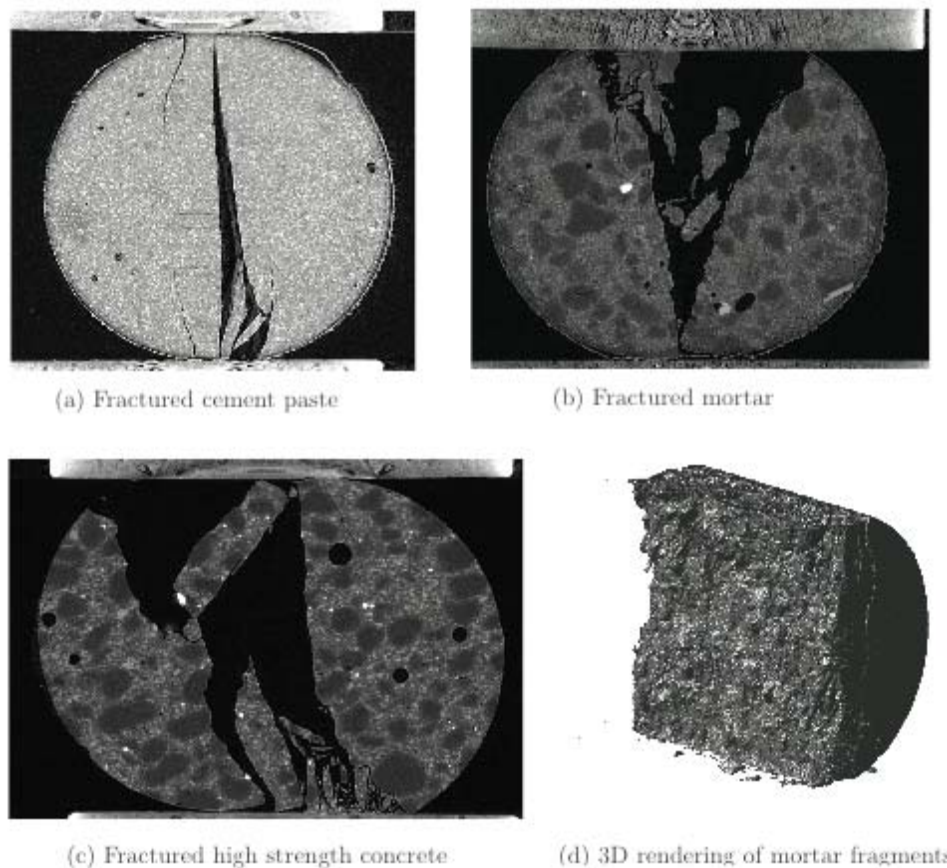
101

(a) Fractured cement paste

(b) Fractured mortar

(c) Fractured high strength concrete

(d) 3D rendering of mortar fragments

Figure 4. Tomographic slices images for different specimens, along with a 3D rendering of a large fragment.

3.1 *3D Image processing*

The vast field of digital image processing provides us with an abundance of tools for quantitative data analysis (e.g. Gonzalez & Woods 2002). In the work described here, we have two objectives: measure the total surface area (within our limits of resolution) of the complex crack system, and count the number of fragments created. Both objectives are realized through simple image segmentation combined with a 3D connectivity analysis.

In this application of image segmentation, we simply wish to isolate the solid material from the background. As the tomographic scan is simply a 3D grayscale intensity image, $I(x,y,z)$, where intensity, I is proportional to x-ray absorption, we can simply employ a threshold-based approach as illustrated in Figure 5. Included in Figure 5 is an intensity histogram that illustrates the selection of the threshold value. We choose the threshold to be the minimum between the two peaks as a way to minimize segmentation error (interpretation of solid to be void, and interpretation of void to be solid.) The result is that voxels having an intensity above the threshold are interpreted to be solid, while all others are interpreted to be void.

The critical step in our image analysis is the object connectivity analysis. In this work we employed a routine developed by Franklin (2006) that allows rapid analysis of large (1000 x 1000 x 1000 voxels

(a) Voxel intensity histogram
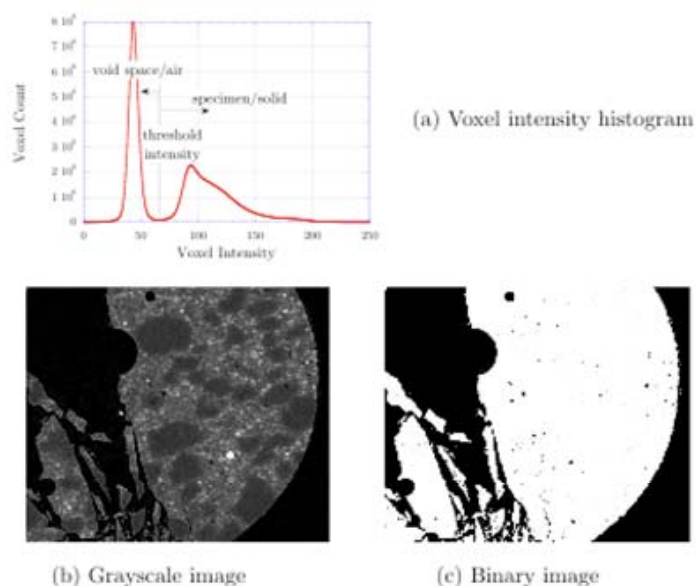
(b) Grayscale image

(c) Binary image

Figure 5. Illustration of binary segmentation process for fractured specimens.

or greater) volumes. The code identifies adjacent voxels as being part of the same object if they share either a face (6 connectivity), or a corner (26 connectivity), as prescribed by the user. Once each object is identified, its volume is measured by simply counting the number of voxels in the object, and its surface area is measured by counting the number of free, or border voxel faces. In this work 6 connectivity was employed. We should note that the tomo-

graphic images described here were on the order of 1000 by 1000 by 700 voxels. In these images we can find tens or even hundreds thousands of objects. However, most of these objects are only a few voxels in size.

Our measurement of the number of discrete fragments created during fracture required an additional step. The connectivity analysis described in the previous paragraph defines objects to be connected no matter how small that connection might be. As a result, two large and otherwise discrete fragments, each containing hundreds of thousands of voxels, are considered to be a single object even if their connection is a single voxel. The nature of the fracture might lead to hundreds of discrete fragments, but the connectivity analysis may tag it as a single object because of inter-fragment contact. To remedy this issue, we employed a 3D "watershed" algorithm that separates objects that are connected, but have identifiable segments (Gonzalez & Wood 2002). The name comes from the 2D analogy with catch basins on a topographic map.

4 EXPERIMENTAL RESULTS

The results of the 3D image analysis can be combined with the measured load-deformation response to calculate the energy associated with fracture of these small specimens. Using the plots shown in Figure 4, the work of load was established by taking the area under the loading curve up to fracture, and subtracting the residual elastic energy manifested in the unloading segment. This quantity represents the energy consumed by fracture. Specific fracture energy can be determined by dividing by the surface area created in the process:

$$G_f = \frac{\Delta U}{\Delta A}$$

(1)

where G_f = specific fracture energy, ; ΔU = the net energy consumed by fracture, and ΔA = the is the overall change in surface area after fracture. Of significance in this work is that our measurement of the change in overall surface area is made from the 3D image analysis described above. As such it includes all the small fragments, intersecting branches and other geometric complexities. The measurement makes no assumptions about the nature of the fracture process zone, and with the resolution of the images, the measurement represents the full complexity of the fracture process.

Table 1 summarizes the fracture measurements as well as the fragmentation analysis. The results are consistent with the long established notion that aggregates introduce a variety of toughening mecha-

Table 1. Analysis of Fracture and fragmentation.

Material	Con-sumed energy mJ	New sur-face area mm^2	Fracture energy J/m^2	Number of frag-ments
Cement paste	5.0	167	30	12
Mortar	11.2	294	38	4041
Ultra high strength mortar	13.0	294	50	3655

nisms. As noted above, the cement matrix of the two conventional materials was identical, so the increase of specific fracture energy can be attributed to the presence of the aggregates, and the disorder they introduce. Indeed, the aggregates cause disorder through crack stopping, redirection, and branching. The presence of the aggregates also introduces weak interfaces that can nucleate a much larger number of initial cracks. The net result is a cement composite that has a 27% higher specific fracture energy, and that produces two orders of magnitude more fragments upon fracture. The high strength cement composite is an interesting case in that it gets its high strength through a very high strength cement matrix, and by reducing or eliminating the interfacial transition zone. Thus it has fewer weak zones where small cracks can nucleate. However, the number of fragments created on fracture is comparable to that of the conventional mortar specimen, suggesting that the presence of aggregates is felt during fracture.

5 CONCLUSION

The work described here, using three-dimensional imaging of fracturing specimens, elucidates the role of microstructural features have on fracture. A simple conclusion we can draw from this work is the critical role the aggregate particles play in the basic fracture processes in the material. While this is by no means a new conclusion, we emphasize it here as it relates to our basic premise that the models we use to represent fracture will be greatly improved by the explicit representation of material heterogeneity in general, and aggregate particles in particular. Current ongoing collaborative work is focused on this specific problem.

ACKNOWLEDGEMENTS

REFERENCES

Bentz, D.P., Quenard, D.A., Kunzel, H.M., Baruchel, J., Peyrin, F., Martys, N.S., and Garboczi, E.J. 2000. Microstructure and transport properties of porous building materials: Three-dimensional X-ray tomographic studies. *Materials and Structures*, 33, 147-153.

Diamond, S., and Landis, E.N. 2007. Microstructural Features of a Mortar as Seen by Computed Tomography. *Materials and Structures*, 40(9), 989-993.

Flannery, B.P., Deckman, H.W., Roberge, W.G., and D'Amico, K.L. 1987. Three-Dimensional X-ray Microtomography. *Science*, 237, 1439-1444.

Franklin, W.R. 2006. CONNECT - find 3D connected components(http://wrfranklin.org/pmwiki/ConnectedComponents)

Gonzalez, R.C., and Woods, R.E. 2002. *Digital Image Processing*, Upper Saddle River: Prentice Hall.

Landis, E.N., Nagy, E.N., Keane, D.T., and Nagy, G. 1999. A Technique to Measure Three-Dimensional Work-of-Fracture of Concrete in Compression. *Journal of Engineering Mechanics*, 125(6), 599-605.

Landis, E.N., Zhang, T., Nagy, E.N., Nagy, G., and Franklin, W.R. (2007). Cracking, Damage and Fracture in Four Dimensions. *Materials and Structures*, 40(4), 357-364.

Lu, S., Landis, E.N., and Keane, D.T. (2006). X-Ray Microtomographic Studies of Pore Structure and Permeability in Portland Cement Concrete. *Materials and Structures*, 39(6), 609-618.

Stock, S.R., Naik, N.K., Wilkinson, A.P., and Kurtis, K.E. 2002. X-ray microtomography (microCT) of the progression of sulfate attack of cement paste. *Cement and Concrete Research*, 32(10), 1673-1675.